2020 IEEE/RSJ International Conference on Intelligent Robots and Systems (IROS)
October 25-29, 2020, Las Vegas, NV, USA (Virtual)

Adaptive Potential Scanning for a Tomographic Tactile Sensor with High Spatio-Temporal Resolution

Hiroki Mitsubayashi[1], Shunsuke Yoshimoto[2], and Akio Yamamoto[2]

***Abstract*— A tactile sensor with high spatio-temporal resolution will greatly contribute to improving the performance of object recognition and human interaction in robots. In addition, being able to switch between higher spatial and higher temporal resolution will allow for more versatile sensing. To realize such a sensor, this paper introduces a method of increasing the sensing electrodes and adaptively selecting the grounding conditions in a tomography based tactile sensor. Several types of grounding conditions are proposed and evaluated using spatio-temporal metrics. As a result, the grounding method based on the location of contact had a good balance of temporal resolution (1 ms) and spatial resolution (only 1.55 times larger than using all electrodes as grounding conditions). When reconstructing dynamic contact data, the proposed method was able to obtain a much higher detailed waveform compared to the conventional method. By using the proposed method as default and switching to other grounding methods depending on the purpose of sensing, a versatile tactile sensor with high spatio-temporal resolution can be made.**

I. INTRODUCTION

Tactile sensors play an important role in the area of robotics and human interface [1]. For example, using tactile sensors to measure the spatio-temporal distribution of pressure greatly contributes to object recognition and robot manipulation. The tactile sensors for these purposes can be realized in many different ways. Gandarias et al. proposed an object recognition system using a high resolution tactile sensor having 1400 pressure sensels [2]. Sudaram et al. proposed a tactile glove for object recognition using matrix type pressure sensors [3]. Tian et al. and Yamaguchi et al. both succeeded in using an image-based tactile sensor, GelSight and Finger Vision respectively, to manipulate robots [4] [5]. As for human interfaces, Zhang et al. proposed a tangible input interface using electric-field tomography and machine learning [6].

In tactile sensors, pressure is most commonly measured by using one of resistance, capacitance, light, and magnetism for detection [7]. Some methods to acquire a distribution from discrete pressure values include arranging detectors in a dense array, and using the intersection in a matrix type fabrication [8]. Using a camera to estimate pressure from displacement is also a widely studied method [9]. However, there is a trade-off between the spatial resolution and the ease of fabrication.

*This work was supported by the Japan Society for the Promotion of Science KAKENHI under Grant JP19H04189.

[1]H. Mitsubayashi is with School of Engineering, The University of Tokyo, 113-8654 Hongo, Tokyo, Japan mitsu@aml.t.u-tokyo.ac.jp

[2]S. Yoshimoto and A. Yamamoto is with the Graduate School of Frontier Sciences, The University of Tokyo, 277-8563 Kashiwa, Chiba, Japan $\{yoshimoto, akio\}$ @$k.u-tokyo.ac.jp$

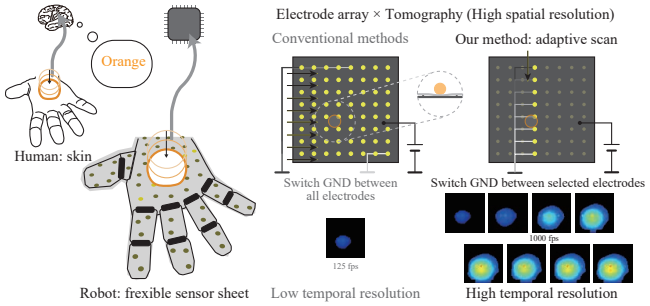

Fig. 1. A tomographic tactile sensor that selects grounding conditions based on the location of touch for achieving high spatio-temporal resolution.

Recently, tomography based methods have been recognized as a means of improving spatial resolution while using less sensor elements [10]–[12]. In the methods, electrodes are generally set on the boundary of a pressure sensitive or conductive continuum used as a detecting layer [13]–[16]. Multiple current patterns are sequentially injected through the layer. For each current pattern, a set of voltage data is acquired from the sensing electrodes. The voltage data are dependent on the pressure applied, and can be used to estimate the location and force of contact. The multiple sets of voltage data are used for interpolation between the electrodes, which results in higher spatial resolution. Also, the continuum layer enables the sensor to detect contact at any given location, whereas most other methods can only detect contact when detector elements are touched.

Given its traits, the tomographic approach seems promising in realizing an easily fabricated and high spatio-temporal resolution tactile sensor. However, large localization errors in the sensor's central region is considered a major drawback. Placing internal electrodes in the detecting region is known to greatly improve the sensor's spatial resolution [17], but the temporal resolution of the sensor decreases due to having more patterns of current injection. For this reason, a tomographic tactile sensor that measures pressure distribution in both high spatial and temporal resolutions has never been implemented.

If a tomographic tactile sensor with high tactile sensing abilities can be realized, a great improvement in the performance of object recognition and robot manipulation can be anticipated. Additionally, being able to switch between higher spatial resolution and higher temporal resolution will allow for more versatile sensing. For example, a robot that adjusts the spatio-temporal resolution of its tactile perception based on the purpose of action can be made.

The purpose of this research is to create a high spatio-temporal resolution tomographic tactile sensor for quantifying the dynamics of objects in motion. To this end, we propose an adaptive potential scanning method for the electromechanically coupled tomographic tactile sensor [18] containing internal electrodes (Fig. 1). The scanning method is based on the trade-off between the spatial and temporal resolutions. Adaptively changing the grounding conditions in an electromechanically coupled tomographic tactile sensor has never been challenged before, and this paper will be a pioneer in the field. The main contributions of this paper are as follows.

1) To address an effective method of potential scanning for tomographic tactile sensors.
2) To develop a high spatio-temporal resolution pressure distribution sensor.
3) To quantify the contact dynamics of objects in motion for upcoming research on object recognition and manipulation.

In the following sections, this paper will first introduce a mathematical model of the tomography method and describe how using informative grounding conditions can result in high spatio-temporal resolution. Then, a simulation will be conducted to discern the promising grounding methods. An algorithm for the proposed grounding methods will be introduced, and a real world experiment will be carried out to compare the proposed methods to the conventional method. The results will be discussed and future works will be stated.

II. Tomography Method with Adaptive Potential Scan

A. Overview

This paper utilizes a tomography method based on contact resistance [18]. The method places a driving layer on top of a grounded probing layer. When force is applied on the driving layer, a current runs from the point of contact to the probing layer. Because the contact resistance between the two layers changes with the amount of force applied, a potential distribution dependent on the location and amount of force is formed in the probing layer. Using electrodes to obtain the potential values and then solving an inverse problem enables the estimation of the location and amount of force.

An abstract flow of the tomography method with newly proposed adaptive potential scan is shown in Fig. 2. Since the potential distribution is dependent on the location of contact, a grounding method adaptive to the contact location may enhance the sensor's overall capabilities. The following section explains this hypothesis in detail using a mathematical formulation of the tomography method. Then, a simulation to compare the proposed method to other grounding methods in both spatial and temporal metrics is conducted.

B. Mathematical Formulation of Tomography Method

The goal of the tomography method is to solve an inverse problem in which the pressure distribution on the detecting region is estimated using voltage data gathered from sensing

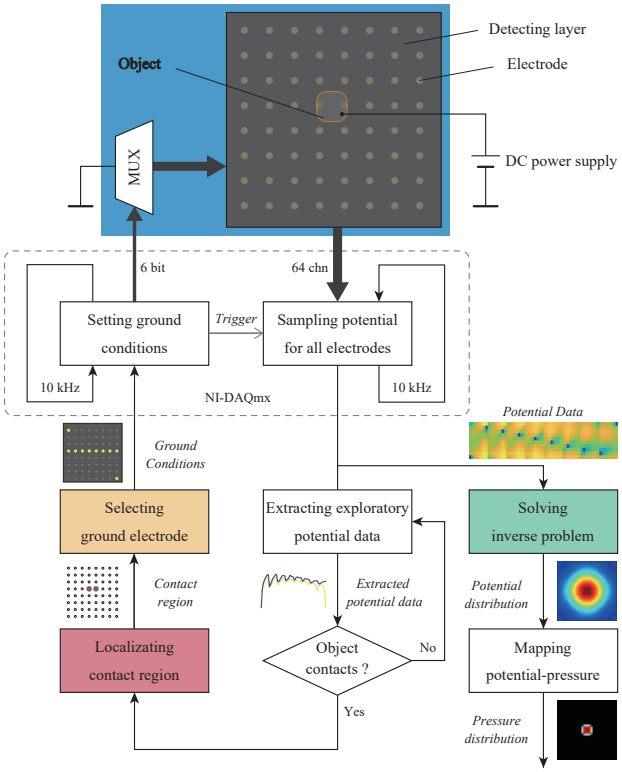

Fig. 2. A flow diagram of the potential scanning procedure.

electrodes. In our previous work [18], the relationship between every contact position ϕ and voltage on the sensing electrodes V is modeled based on Maxwell's equation. The modeled Jacobian matrix $J_{i,k}$ is represented as follows:

$$J_{i,k} = \frac{\delta V_i}{\delta \phi_k}; \quad i = 1...ML; \quad k = 1...K, \tag{1}$$

where M is the number of electrodes, L is the number of GND conditions, and K is the number of elements in the mesh representing the detecting region. One can increase the rank of the Jacobian by adding more sensing electrodes and GND conditions, which will provide more information to solve the inverse problem. However, increasing the number of GND conditions will require the sensor more time to complete a single potential scan, resulting in a lower temporal resolution.

Our novel method proposed in this paper is to reduce the GND conditions in a potential scan by taking notice of the fact that GND conditions which spread similar potential distributions inside the detecting region give little information to solve the inverse problem. By increasing the number of sensing electrodes and grounding only the electrodes that give abundant information to the Jacobian matrix, a tomographic tactile sensor with high spatial and temporal resolution can be made. Grounding the electrodes near the point of contact spreads potential distributions that are more different compared to grounding electrodes far from the point of contact. This means grounding the electrodes adaptivley to the point of contact will give more

information to solve the inverse problem. By selecting L_s GND conditions, the temporal resolution Δt of the sensor is represented as follows:

$$\Delta t = \frac{L_s}{f_{sw}}, \tag{2}$$

where f_{sw} is GND switching frequency. It is clear that using less GND conditions results in a higher temporal resolution.

To solve the inverse problem using data from only the selected GND conditions, a new Jacobian submatrix J_s using elements of the selected GND conditions from the Jacobian matrix in (1) should be made. The Tikhonov regularization is then used to make a regularized inverse matrix for J_s, and the solution to the inverse problem can be calculated as follows.

$$\phi = ({J_s}^T J_s + \lambda I)^{-1} {J_s}^T V_s, \tag{3}$$

where λ is a hyperparameter, I represents an identity matrix, V_s is the voltage data gathered from the selected GND conditions, and the inverse matrix for J_s is an $L_s \times L_s$ matrix. The Jacobian matrix in (1) is calculated once, and the regularized inverse matrix for its submatrix J_s is calculated for every combination of selected GND conditions. Finally, the estimated potential distribution can be converted to the pressure distribution as explained in [18].

C. Simulation to Discern the Informative GND Conditions

The potential distribution inside the detecting region is dependent on the relative positions of the GND electrode and the contact area. To test our hypothesis of adaptive potential scanning, we reconstructed the potential distribution for each of the grounding methods and contact area shown in Fig. 3. *Around*, *CoP line*, and *Point* utilize adaptive scanning, while the others do not. The *Random* conditions were tested 3 times each for the grounding of both 8 and 16 random electrodes.

Potential data used in the simulation were given using Maxwell's equation to exclude any external factors that may affect the results, such as the contact state between the detecting layer and the electrodes. The simulations were executed on a 160 mm $\times$ 160 mm square mesh made of triangular elements. Each of the 160 mm sides were split into 40 even elements, creating a 3200 element mesh. 64 electrodes were set inside the mesh in 20 mm intervals.

The reconstructed potential distributions were evaluated from both spatial and temporal perspectives. Since the spatial resolution of the reconstructed potential distribution cannot be calculated precisely, the half-value width for the single contact condition was used instead as a reference. In contrast, the temporal resolutions were calculated using 2. The scores of all GND conditions are shown in table I. In order to analyze the trade off between spatial and temporal metrics, the evaluation values were normalized, then added together with the weight of each being the horizontal axis. The left edge of the graph represents the evaluation score when considering only spatial resolution. The right edge of the graph represents the same for temporal resolution.

The method *All*, which switches the grounding conditions between all 64 electrodes obviously had the highest spatial resolution and the lowest temporal resolution. On the other hand, the methods *Around*, which switch the grounded electrodes around the area in contact, and *CoP line*, which switch the grounded electrodes in a straight line near the area in contact, seemed to have good overall evaluation scores. The methods *Edge* and *V line* both ground electrodes in a straight line similar to *CoP line*, but the results were poor. This seems appropriate since the potential distribution becomes more similar the farther the grounding electrodes are from the area in contact. The methods *Boundary*, which switch the grounded electrodes around the edges of the detecting region, and *Random 16*, which switch the grounding conditions between 16 electrodes, did not have high spatial resolution despite having a larger number of grounding conditions. Finally, the method *Point* which grounded the 4 corners and 2 electrodes nearest to the area in contact had the worst spatial resolution of all the methods.

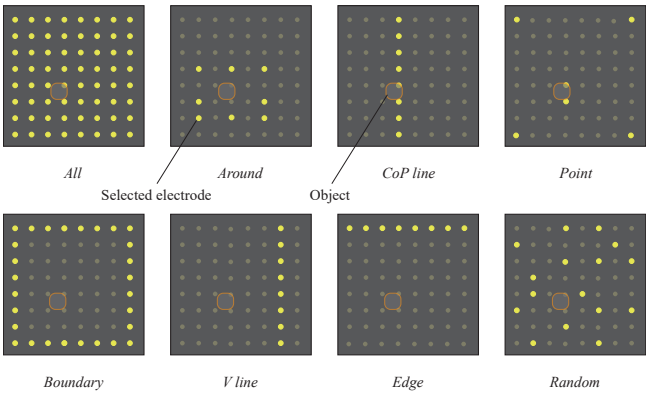

Fig. 3. The GND conditions and contact area used in the simulation.

TABLE I
SCORES OF ALL GND CONDITIONS.

Conditions	Spatial metrics [mm]	Temporal metrics [ms]
All	32.2	6.4
Around	45.6	0.80
CoP line	50.0	0.80
Point	62.2	0.60
Boundary	46.3	2.80
V line	60.0	0.80
Edge	57.8	0.80
Random 16	49.0	1.60
Random 8	56.6	0.80

From the results, it seems reasonable to select the adaptive grounding conditions using *Around* or *CoP line* as default. For higher spatial resolution scanning, the conventional *all* method may be used. For higher temporal resolution scanning, the method *point* may be used.

D. Adaptive Potential Scanning

Because the two proposed grounding methods, i.e. *Around* and *CoP line*, choose GND conditions based on the center of pressure, exploratory potential data are first gathered by selecting two corner electrodes as the ground. The electrode with the highest sum in voltage is determined as the center of contact, and all electrodes within $\alpha\%$ of the highest sum

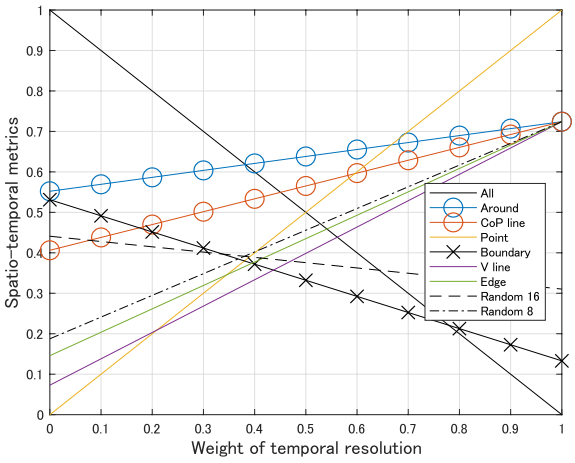

Fig. 4. The weighted score of all GND conditions.

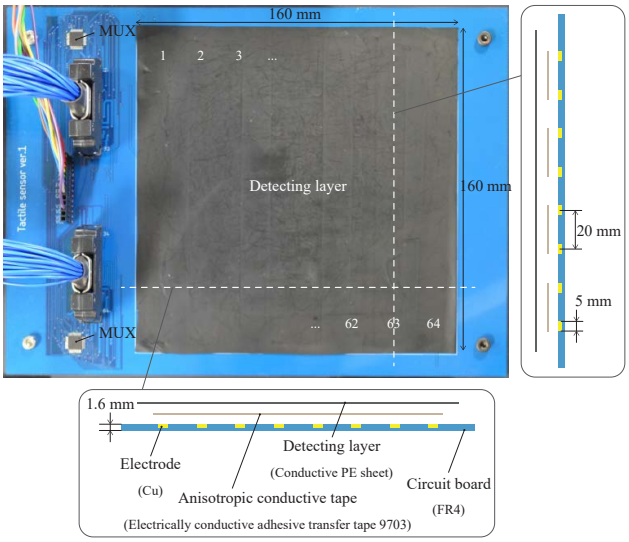

Fig. 5. The structure of the fabricated sensor.

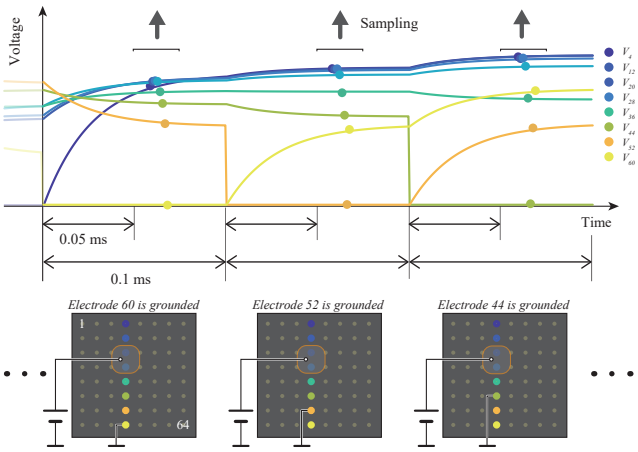

Fig. 6. Switching ground conditions and gathering voltage data.

is considered to be electrodes in contact with the target of observation. α can be changed depending on the sensitivity and the detector material. In our experiment, α was set to 95. Next, the GND conditions are selected from the shape of the electrodes in contact.

As for the *Around* method, the electrodes along the boundary of the contact region is grounded. For multiple contact conditions, it would be best to bound both contact areas separately. However, this is difficult to achieve, so we simply set the bounding box for the estimated overall contact region and grounded the electrodes at the corner and midpoint of the rectangular sides.

As for the *CoP line* method, the shape of the contact region is considered to select a grounding line. First, the principal direction of the contact region is calculated and is categorized into eight directions on the detecting layer. Then, the electrodes close to the detected line are selected. If the number of electrodes is smaller than the preset number of GND conditions, an additional line which is perpendicular to the principal line is used for selecting the remaining ground conditions.

E. Fabrication of the Sensor

In this paper, 64 electrodes were embedded in a 160 mm $\times$ 160 mm circuit board, as shown in Fig. 5. The electrodes have a diameter of 5 mm and were placed in 20 mm intervals. Electrodes 1 and 64 were used for sparse potential data. Two ADG732BSUZ multiplexers, which control 32 channels each, were used to ground an arbitrary electrode in the circuit board. A polyethylene sheet containing carbon particles was used as the detecting layer. The sheet has a surface resistance of 10 kΩ/sq, and was attached to the electrodes using anisotropic conductive tape. The anisotropic tape has an insulating resistance of 3.4×10^{14} Ω/sq in the plane of the adhesive and a contact resistance of under 0.3 Ω, meaning no notable energy is lost as current runs perpendicularly from the detecting layer to the sensing electrode. We assume that the target object is a conductive material and connected to a DC power supply. The DA converter NI-PXIe-6739 from National Instruments was used to send signals to the multiplexer that switches the grounding conditions at a rate of 10 kHz. The ground was switched between the 2 corner and 8 selected ground conditions for a reconstruction rate of 1 kHz. The AD converter NI PXIe-6355 was used to gather voltage data from the sensing electrodes. NI PXIe-6355 has a multiplexed analog input with a maximum combined sampling speed of 2.86 MSamples/sec. This means that that sampling of all 64 electrodes happens in a span of 22.3 μs, which is 4.48 times faster than the switching rate of the grounding electrodes. The two modules were connected to the chassis NI PXIe-1073 and were controlled by LabVIEW. When a voltage induced object touches the detecting layer, a current runs in the layer from the point of contact to the selected ground electrode. 64 channel voltage data can be acquired from the sensing electrodes as shown in Fig. 6. In this paper, the output maps were reconstructed offline.

III. Experiment

A. Reconstructing Pressure Distribution with Static Objects

For the comparison of spatial distributions, the two proposed grounding methods, i.e. *CoP line* and *Around*, and the methods *All* and *V line* were used to acquire voltage data. Data on a single point contact using a 100 g weight, a double point contact using a 50 g and a 100 g weight, and a wide area contact using a spanner were collected for all 4 grounding methods. 4.5 V were externally applied to each of the objects to spread a potential distribution inside the detecting layer. The grounded electrodes and reconstructed results for each object and grounding method are shown in Fig. 7. All the maps only show data above the same threshold level. Note that because the threshold level was set so the 50 g weight would be visible in *All*, the maps in the single point contact and wide area contact are widely spread out. The two proposed methods *Around* and *CoP line* correctly displayed the center of pressure in the single point contact, whereas *V line* displayed the center to the right of the true position.

In the two point contact, none of the methods except *All* could create a potential distribution that can discern the two objects as separate. However, the two proposed methods did indicate the location of the 50 g weight better than the method *V line*.

In the wide area contact, the methods *All*, *Around*, and *CoP line* made potential distributions that correctly display the center of pressure. The *All* method also represented the size of the spanner the best. However, the methods could not discern the direction of the spanner. *V line* could not indicate direction, center of pressure, or size correctly.

B. Reconstructing Dynamic Data

Dynamic data of an orange and a spanner being dropped on the detecting region were acquired at a 10 kHz sampling rate using the grounding methods *All* and *CoP line*. The method *Around* was not tested because the results in III-A suggest the outcome to be similar to *CoP line*. The temporal resolution of the two methods are as shown in Table I. The orange weighed 43.7 g and had a resistance of around 200 kΩ. The spanner weighed 8.9 g and had a resistance of 0.3 Ω. The voltage values at the center of pressure were recorded for each of the reconstructed potential distributions. Note that the voltage values can be converted into pressure values using the method in [18], but the process was omitted since it would not notably affect the results. The top line in Fig. 8(a) shows the transition of the pressure value of the dropped orange for the *CoP line* method. A time series of the reconstructed pressure map is shown for a section of the data. The bottom line shows the pressure value for *All*. Fig. 8(b) shows the results for dropping the spanner. It is clear that the *CoP line* method captures more information on the bouncing sequence due to its higher temporal resolution.

C. Discussion

Data acquired from the proposed methods were used to reconstruct a distribution that correctly displays the center of pressure for a single target. However, the methods could not discern two separate targets. A derivation of the *Around* method that grounds the electrodes around each of the contact locations may improve the performance of multiple contact differentiation. Using the *All* method for multiple target observations might also be a solution.

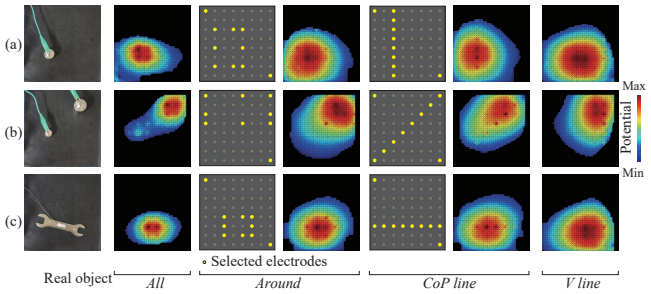

Fig. 7. Result of pressure reconstruction. (a) single contact condition, (b) double contact condition, and (c) areal contact condition.

The results in the reconstruction of dynamic data suggest that the proposed method does in fact enable the sensor to discern higher frequencies of movement compared to the previous grounding method where all electrodes were grounded. Since human are said to have a tactile temporal resolution of about 1 ms [1], the proposed method discerns motion undetectable by humans. Using the *Point* method will enable even higher temporal resolution scanning. Quantifying the localization errors of the sensor using each grounding method may be an effective way to further prove the validity of the proposed method. Also, placing a driving layer on the detecting layer will enable the detection of non-conductive objects that were not measured in this paper [18].

An apprehension of the proposed method is that latency was inevitable when calculating the center of pressure from exploratory potential data and continuously setting the grounding conditions. To evade this problem, we preset the grounding conditions so that no calculation was needed in the sensing process. A method to roughly determine the center of pressure and set grounding conditions accordingly with minimal latency is needed for the proposed method to accommodate to real-world sensing. Some other limitations of the method include not being able to accurately detect multiple touch, and that the target of observation must be conductive and electrically connected. The former limitation may be overcome by simultaneously grounding multiple electrodes near the area of contact. This may give more information on the multiple locations of touch. The latter limitation can be overcome simply by placing a driving layer on top of the existing probing layer.

IV. Conclusions

This paper presented the results on a method of potential scanning where the grounding conditions are determined adaptive to the center of pressure. Grounding the electrodes in a straight line near the center of pressure and around the center of pressure was found to be an effective and efficient grounding method for the tomographic tactile sensor. A

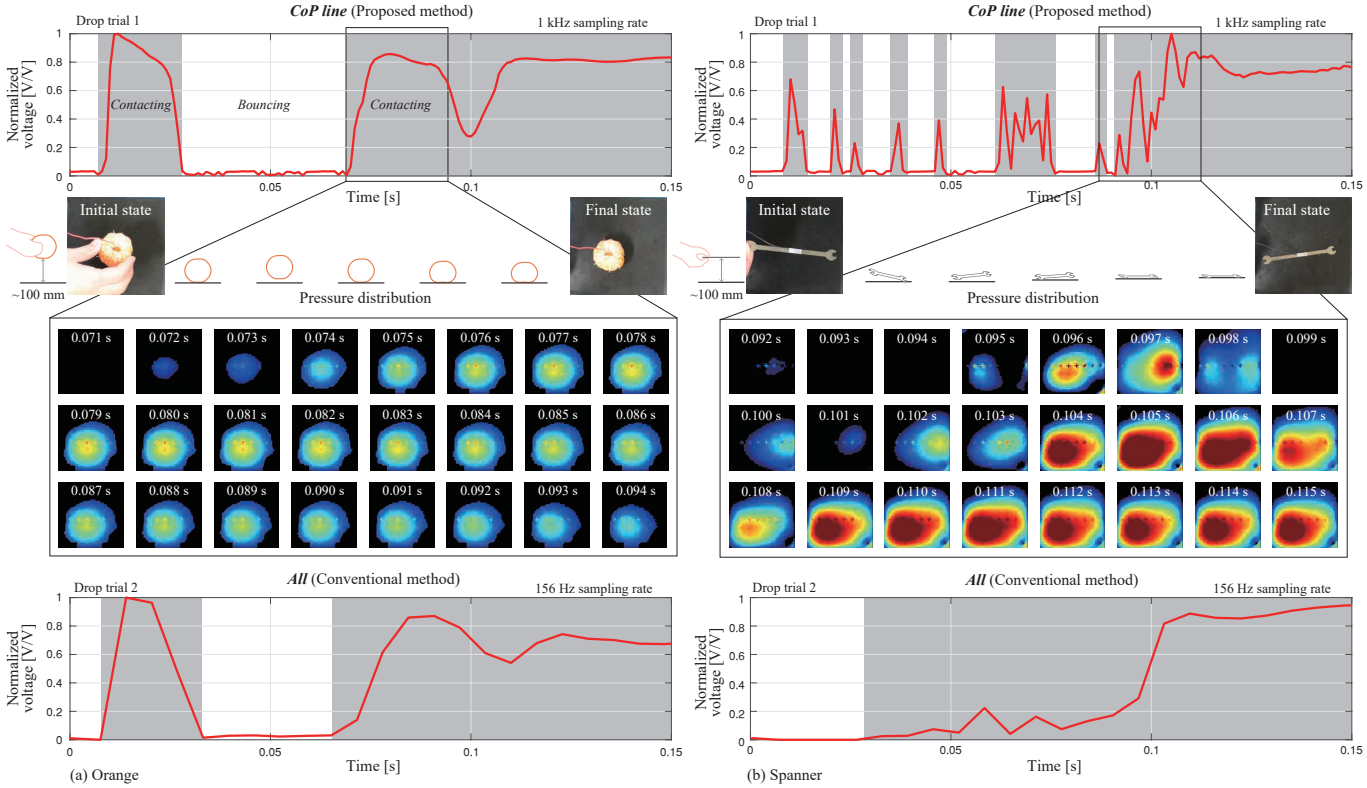

Fig. 8. Result of pressure response for *CoP line* method and all. (a) falling orange and (b) falling spanner.

temporal resolution of 1 ms was achieved with the method, which enabled the detection of high frequency movement. In addition, it became clear that the conventional method of grounding all electrodes could be used in the same sensor structure for higher spatial resolution scanning. Switching between grounding methods can be applied to robots that adjust the spatio-temporal resolution of their tactile perception depending on the purpose of their actions. This will result in a more versatile object recognition system.

REFERENCES

[1] R. S. Dahiya, G. Metta, M. Valle, and G. Sandini, "Tactile Sensing-From Humans to Humanoids," *IEEE Trans. Robot.*, vol. 26, no. 1, pp. 1–20, 2010.

[2] J. M. Gandarias, A. J. Garcia-Cerezo, and J. M. Gomez-de Gabriel, "CNN-Based Methods for Object Recognition with High-Resolution Tactile Sensors," *IEEE Sens. J.*, vol. 19, no. 16, pp. 6872–6882, 2019.

[3] S. Sundaram, P. Kellnhofer, Y. Li, J.-Y. Zhu, A. Torralba, and W. Matusik, "Learning the Signatures of the Human Grasp Using a Scalable Tactile Glove," *Nature*, vol. 569, no. 7758, pp. 698–702, 2019.

[4] S. Tian, F. Ebert, D. Jayaraman, M. Mudigonda, C. Finn, R. Calandra, and S. Levine, "Manipulation by Feel: Touch-Based Control with Deep Predictive Models," in *Proc. 2019 International Conference on Robotics and Automation*, 2019, pp. 818–824.

[5] A. Yamaguchi and C. G. Atkeson, "Combining Finger Vision and Optical Tactile Sensing: Reducing and Handling Errors While Cutting Vegetables," in *Proc 2016 IEEE-RAS 16th International Conference on Humanoid Robots*, 2016, pp. 1045–1051.

[6] Y. Zhang, G. Laput, and C. Harrison, "Electrick: Low-Cost Touch Sensing Using Electric Field Tomography," in *Proc. 2017 SIGCHI Conference on Human Factors in Computing Systems*, 2017, pp. 1–14.

[7] Tiwana, Mohsin I., Stephen J. Redmond, and Nigel H. Lovell. "A review of tactile sensing technologies with applications in biomedical engineering," Sens. Actuators A Phys., Vol. 179, pp. 17–31, 2012.

[8] M. Shimojo, T. Araki, A. Ming, and M. Ishikawa, "A High-Speed Mesh of Tactile Sensors Fitting Arbitrary Surfaces," *IEEE Sens. J.*, vol. 10, no. 4, pp. 822–830, 2010.

[9] W. Yuan, S. Dong, and E. H. Adelson, "Gelsight: High-Resolution Robot Tactile Sensors for Estimating Geometry and Force," *Sensors*, vol. 17, no. 12, p. 2762, 2017.

[10] M. Cheney, D. Isaacson, and J. C. Newell, "Electrical Impedance Tomography," *SIAM REV.*, vol. 41, no. 1, pp. 85–101, 1999.

[11] H. Lee, D. Kwon, H. Cho, I. Park, and J. Kim, "Soft Nanocomposite Based Multi-Point, Multi-Directional Strain Mapping Sensor Using Anisotropic Electrical Impedance Tomography," *Sci. Rep.*, vol. 7, 2017.

[12] S. Russo, S. Nefti-Meziani, N. Carbonaro, and A. Tognetti, "A Quantitative Evaluation of Drive Pattern Selection for Optimizing EIT-Based Stretchable Sensors," *Sensors*, vol. 17, no. 9, p. 1999, 2017.

[13] Y. Kato, T. Mukai, T. Hayakawa, and T. Shibata, "Tactile Sensor Without Wire and Sensing Element in the Tactile Region Based on EIT Method," in *IEEE Sens.*, 2007, pp. 792–795.

[14] D. Silvera-Tawil, D. Rye, M. Soleimani, and M. Velonaki, "Electrical Impedance Tomography for Artificial Sensitive Robotic Skin: A Review," *IEEE Sens. J.*, vol. 15, no. 4, pp. 2001–2016, 2015.

[15] T. N. Tallman, S. Gungor, K. W. Wang, and C. E. Bakis, "Tactile Imaging and Distributed Strain Sensing in Highly Flexible Carbon Nanofiber/Polyurethane Nanocomposites," *Carbon*, vol. 95, pp. 485–493, 2015.

[16] S. Liu, J. Jia, Y. D. Zhang, and Y. Yang, "Image Reconstruction in Electrical Impedance Tomography Based on Structure-Aware Sparse Bayesian Learning," *IEEE Trans. Med. Img.*, vol. 37, no. 9, pp. 2090–2102, 2018.

[17] H. Lee, K. Park, J. Kim, and K. J. Kuchenbecker, "Internal Array Electrodes Improve the Spatial Resolution of Soft Tactile Sensors Based on Electrical Resistance Tomography," in *Proc 2019 International Conference on Robotics and Automation*, 2019, pp. 5411–5417.

[18] S. Yoshimoto, Y. Kuroda, and O. Oshiro, "Tomographic Approach for Universal Tactile Imaging with Electromechanically Coupled Conductors," *IEEE Trans. Ind. Electron.*, vol. 67, no. 1, pp. 627–636, 2018.